World Academy of Science, Engineering and Technology
International Journal of Aerospace and Mechanical Engineering
Vol:19, No:8, 2025

Designing an Electronic Power Supply using Maximum Power Point Tracking for a CubeSat

Nayim Ali, Anwar Ali

***Abstract*—**This paper looks at six maximum power point tracking techniques, including three conventional tracking methods (perturb and observe, incremental conductance, and constant voltage) and three intelligent tracking methods (fuzzy logic control, particle search optimization, and an artificial neural network). Using a solar module with an output voltage of 4.4 V and current of 400 mA at maximum power provides 1.76 W. The electronic power supply is designed to be fitted to one face of a 1U CubeSat chassis. Simulink was used to simulate the electronic power supply and calculate the efficiencies of the DC-DC converter and maximum power point tracking. The artificial neural network was determined to be the most efficient algorithm, with a DC-DC converter efficiency of 92.10% and a maximum power point tracking efficiency of 98.57%. This supplied an output power of 1.598 W from the electronic power supply to be used in the CubeSat system.

***Keywords*—**Fuzzy logic, maximum power point tracking, neural network, particle swarm optimization.

I. Introduction

PHOTOVOLTAIC (PV) cells are common power sources for small dimension satellites orbiting within low Earth orbit. Therefore, the electronic power supply (EPS) is an essential component of the satellite allowing prolonged deployment. CubeSats specification satellites follow standardized sizing using U as a unit [2]; 1U is the smallest size, designated for cube shaped satellites with dimensions of 10 cm on all lengths and a maximum mass of 2 kg. Smaller and lighter components are ideal due to the limited volume and weight [3].

The electronic power supply (EPS) is an essential component of the satellite as it powers the system allowing prolonged deployment. Solar modules for a single CubeSat face can have two small PV cells fitted to generate around 1.76 W of power depending on cell specifications [4]. Conditions such as temperature and irradiance impact the cells' voltage and current output as the solar module's angle to the sun changes during rotation. This affects the power-voltage (P-V) relationship of the PV cell, which changes the maximum power point (MPP). To ensure the MPP is obtained from the cell, techniques for maximum power point tracking (MPPT) are implemented using an onboard microcontroller or analogue equivalent [5]. MPPT algorithms can control a switch mode DC-DC converter, altering the voltage and the current draw from the PV cell. Switch mode power supplies (e.g., buck and boost converters) are more efficient than linear voltage regulators, which is important due to the low power generated from the PV cells.

Nayim Ali and Anwar Ali are with Faculty of Science and Engineering, Swansea University, Bay Campus, Swansea UK (e-mail: anwar.ali@swansea.ac.uk).

The MPPT methods evaluated in this paper include conventional MPPT and intelligent MPPT [6]. Perturb and observe (P&O) and incremental conductance (INC) are two MPPT techniques which fall under conventional tracking; the algorithms actively search for the MPP. A further conventional tracking method is the constant voltage (CV) technique, despite not being a true tracking algorithm - only a reference voltage is analysed to determine the MPP. Conventional MPPT are cheaper to implement and less power intensive.

Intelligent MPPT algorithms include fuzzy logic control (FLC), particle swarm optimization (PSO) and an artificial neural network (ANN). Intelligent algorithms vary in their accuracies caused by difference in approach but are more reliable and more accurate than conventional methods. However, they are usually more expensive and require more computation power compared to conventional tracking.

This paper aims to simulate and analyse the six described MPPT techniques to identify the most efficient technique which could be implemented on a CubeSat EPS. Firstly, the methodology for the EPS then each MPPT technique will be outlined; followed by analysis of simulation results; and concluding with a comparison of MPPT methods. Simulations will be conducted in Simulink, which is a software packaged with MATLAB [7].

The outcome of the paper is that the best tracking method was ANN, with P&O second. This is due to high MPPT and DC converter efficiency. Additionally, ANN supports the theoretical best duty cycle for MPPT calculated using the parameters described in this paper.

II. EPS Methodology

The EPS is designed for a specific model of solar cell. This EPS uses a boost converter to convert voltage from 4.4 V to 14 ± 2 V through the following methods.

A. Solar Module Specifications

The solar cells are modelled similarly to that of a CESI CTJ30 triple-junction solar cell [8], which has a size of 6.9x3.9 cm^2. This means that two cells can be fitted onto one side of a 1U CubeSat chassis like that shown in Fig. 1. The solar module, comprised of two CTJ30 cells, will be modelled as a current source in parallel with a diode as depicted in Fig. 2. This model includes the photocurrent from the PV cell I_{PV}, current flowing through the diode I_{D1}, the shunt resistance R_{sh} and the series resistance R_s of the cell. The output of the PV model is the voltage V and current I.

Fig. 1 Two Solar Cells Forming a Solar Module on One Face of a CubeSat [9]

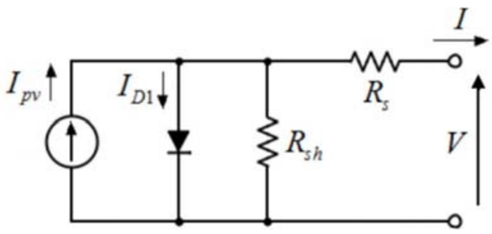

Fig. 2 Equivalent Model of a Photo-Voltaic Cell [4]

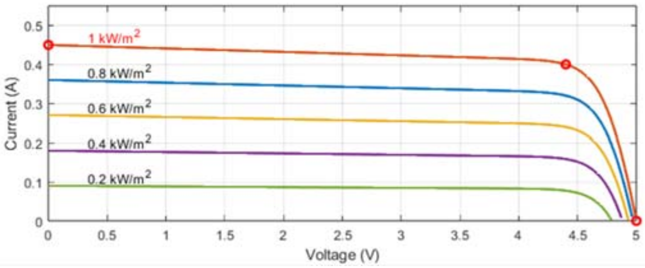

Fig. 3 Current-Voltage Curve of PV Cell at Irradiance 200 Wm^{-2}, 400 Wm^{-2}, 600 Wm^{-2}, 800 Wm^{-2}, 1000 Wm^{-2}, and the Corresponding MPP

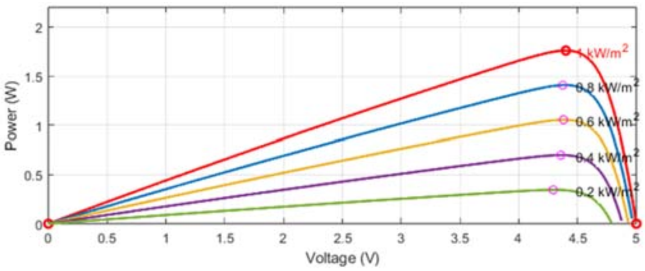

Fig. 4 Power-Voltage Curve of PV Cell at Irradiance 200Wm^{-2}, 400 Wm^{-2}, 600 Wm^{-2}, 800 Wm^{-2}, 1000 Wm^{-2}, and the Corresponding MPP

At MPP, the voltage V_{mp}, will be modelled as 4.4 V and the current I_{mp}, is modelled as 400 mA. This gives an MPP of 1.76 W. The open-circuit voltage is assumed to be 5 V, and the closed-circuit current is assumed to be 450 mA. Using Simulink, the current-voltage and power-voltage curves of the PV module can be plotted.

Fig. 3 shows that as the irradiance increases, the current increases with little change in voltage. Fig. 4 depicts the change in the P-V curve when irradiance changes. This highlights that MPP changes with irradiance. The CubeSat will be rotating as it orbits, which will cause the irradiance to decrease as the solar module faces away from the sun and increase as it faces towards it.

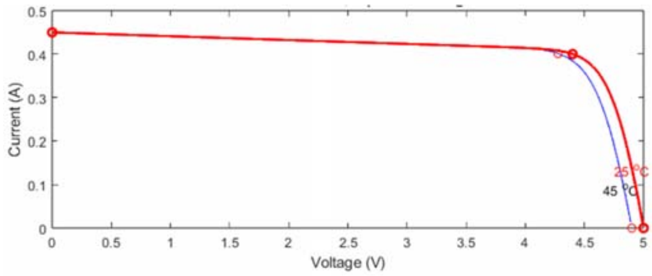

Fig. 5 Current-Voltage Curve of PV Cell at Temperatures 25 °C, 45 °C, and the Corresponding MPP

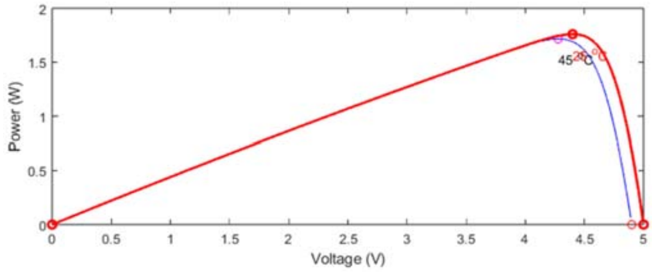

Fig. 6 Power-Voltage Curve of PV Cell at Temperatures 25 °C, 45 °C, and the Corresponding MPP

Fig. 5 shows that increasing the temperature causes a drop in the voltage at MPP while Fig. 6 depicts the change in the P-V curve at the two temperatures, highlighting the shift in the MPP.

B. Designing the Boost Converter with LTspice

The desired output for the CubeSat EPS is 14 ± 2 V. To reach this output voltage, the voltage of the PV will be stepped up using a boost converter. The boost converter uses a MOSFET, which dissipates power when switching from on and off, therefore, a suitable switching frequency must be selected so that too much power is not wasted from the MOSFET when switching. The chosen switching frequency is 25000 Hz, which is above auditory range.

Using the conservation of energy, a power of 1.76 W and a voltage of 14 V gives a current of 126 mA. So, the load chosen for the boost converter is 110 Ω using Ohm's law. The modelling of the boost converter is done by following Hart [10] and the model is initially constructed using LTspice [11]. The duty cycle D is calculated using (1):

$$D = 1 - \frac{V_s}{V_o} \tag{1}$$

where, V_S is the input voltage of the converter and V_O is the converter's output voltage. Using 4.4 V as V_S and 14 V for V_O a duty cycle of 0.686 is calculated. This duty cycle is equivalent to the MOSFET being turned on for 27 µs out of a period of 40 µs for the frequency of 25000 Hz. The duty cycle is used to calculate the minimum inductance L_{min} needed for the DC converter. This is done using (2):

$$L_{min} = \frac{D(1-D)^2 R}{2f} \tag{2}$$

where R is the load resistance and f is the frequency of the converter. Using 110 Ω for load resistance and 25000 Hz for frequency gives a value of 149 µH for the inductor. To allow a margin of safety, the inductor used in the DC converter has an inductance 20% greater than L_{min}. This gives an inductance of 180 µH. In LTspice, the peak current rating of the inductor selected in the converter is 1.1 A.

To ensure that the boost converter operates in continuous conduction mode, the minimum current in the inductor should not fall below 0 A. The average inductor current I_L is calculated using (3):

$$I_L = \frac{V_S}{(1-D)^2 R} \tag{3}$$

This gives an average current of 405 mA. The change in inductor current Δi_L is then calculated to be 337 mA using the following:

$$\Delta i_L = \frac{V_S D}{Lf} \tag{4}$$

Using (3) and (4), the minimum and maximum inductor currents can be calculated by adding and subtracting half of the change in current respectively. This is demonstrated in (5) and (6):

$$I_{min} = I_L - \frac{\Delta i_L}{2} \tag{5}$$

$$I_{max} = I_L + \frac{\Delta i_L}{2} \tag{6}$$

This gives a minimum inductor current I_{min} of 67.5 mA, which is above the threshold of 0 A. The maximum inductor current I_{max} is 742 mA, which is within the maximum current rating of the chosen inductor in LTspice.

A capacitor is placed in parallel to the load to reduce the ripple in the output voltage. The required capacitance can be calculated using (7):

$$C \geq \frac{D}{R\left(\frac{\Delta V_O}{V_O}\right)f} \tag{7}$$

To limit the output voltage ripple to 1%, ΔV_O is 0.14 V. This requires a capacitance greater than 24.9 µF, so a capacitor of 33 µF with a voltage rating of 35 V is chosen in LTspice.

Fig. 7 shows the complete boost converter circuit in LTspice using the components previously derived. The diode used is a Schottky diode. The circuit was simulated in LTspice and found to operate within the continuous conduction mode as desired. This boost converter is a key section of the EPS.

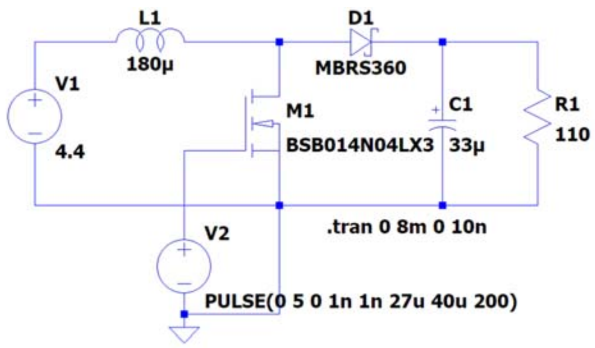

Fig. 7 Boost Converter Circuit Diagram in LTspice

C. Designing the EPS in Simulink

The boost converter circuit in Fig.7 is adapted and reproduced in Simulink which is depicted in Fig. 8. The completed EPS has various changes and additions.

Additions to the circuit include voltmeters and current meters connected to the circuit to measure input voltage V_{PV}, input current I_{PV}, output voltage V_{out} and output current I_{out}. Simulink's 'Scope' is used to display this data.

The model in Simulink (Fig. 8) is changed from the LTspice model (Fig. 7). This change is the gate signal for the MOSFET, which is now controlled using a MATLAB function containing the MPPT algorithms. The algorithm is outputted from the Simulink 'From' block labeled 'Gate'. The MPPT algorithms operate periodically every 100 ms. This allows the power tracking to be responsive when finding the MPP but not too power intensive.

A further addition in Fig. 8 is the Simulink 'PV Array' block and smoothing capacitor C_{PV} in parallel. The PV Array labelled 'Solar Cells' is set with the parameters of the CTJ30 cell previously described and has inputs for irradiance and temperature. This will act as the solar cell module for the simulation.

C_{PV} was chosen as 4 mF. This capacitance is potentially oversized, negatively affecting the efficiency of the boost converter. The capacitor is not suited to the circuit and detrimentally stores and releases energy, reducing EPS efficiency. This effect is present during all simulations in this paper and causes the output power to ripple during certain periods.

D. EPS Efficiency

To calculate the efficiency of the MPPT algorithms, two values need to be looked at. The efficiency of the MPPT algorithm η_{MPPT} and the efficiency of the boost converter η_{DC}, which are calculated using (8) and (9):

$$\eta_{MPPT} = \frac{P_{in}}{P_{mp}} \times 100\% \tag{8}$$

$$\eta_{DC} = \frac{P_{out}}{P_{in}} \times 100\% \tag{9}$$

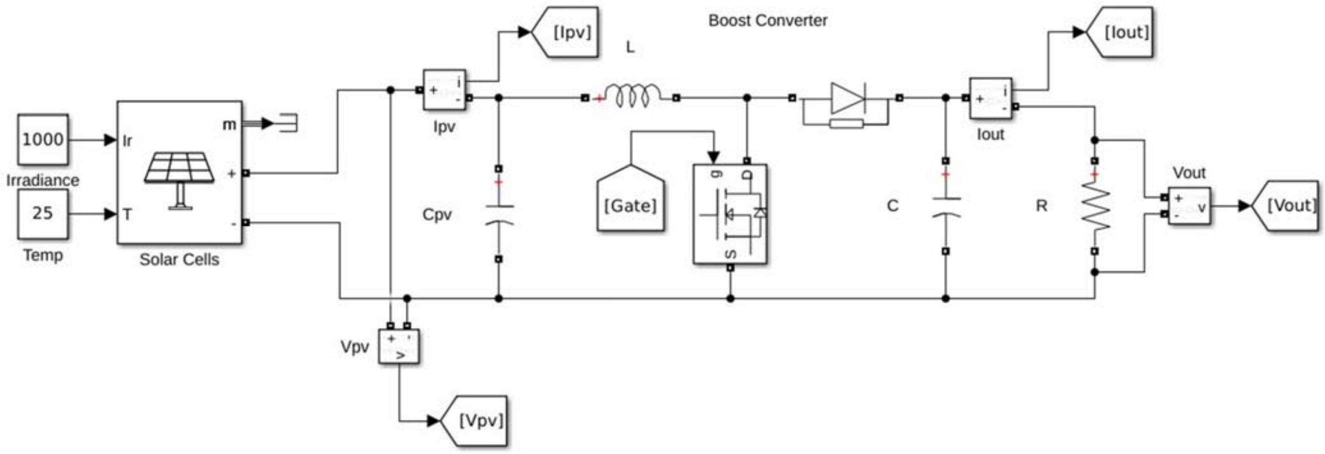

Fig. 8 EPS Circuit Diagram in Simulink

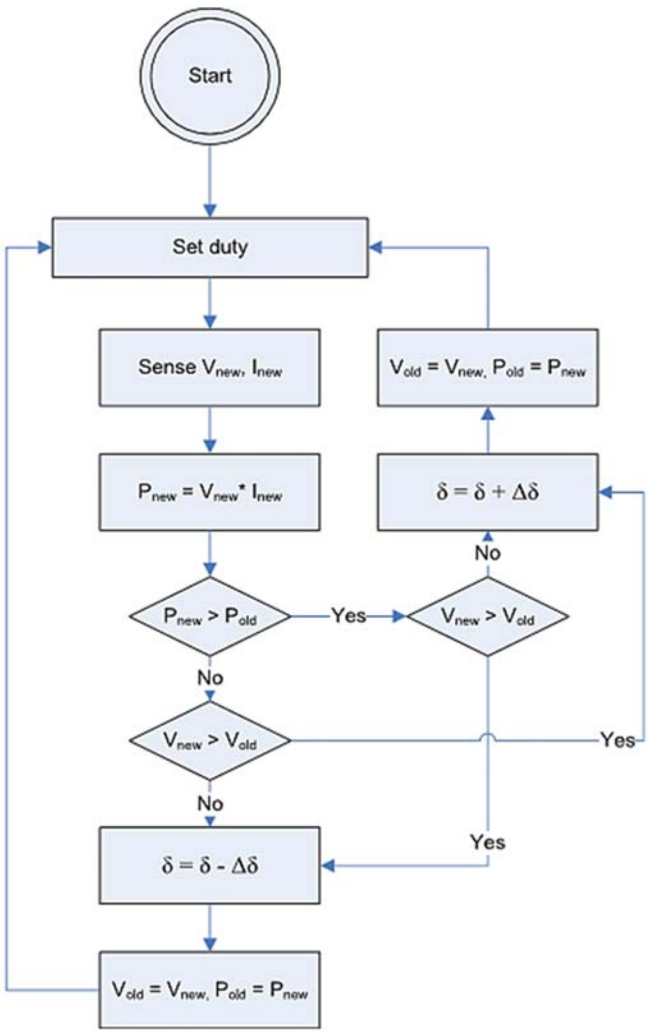

Fig. 9 Flowchart of Perturb and Observe MPPT [12]

These efficiency metrics will be used to compare the six different algorithms to identify the most efficient MPPT.

III. MPPT METHODOLOGY

A. Perturb and Observe

The flowchart by Verma et al. [12], as seen in Fig. 9, shows the P&O algorithm. The algorithm measures the voltage and current of the PV, then it calculates the power. If power increased from the previous measurement, and voltage also increased, then the duty cycle is reduced by delta. Otherwise, if the voltage decreased, then the duty cycle is increased by delta. Similarly, if power decreased and voltage decreased then duty is reduced by delta or if the voltage increased then the duty is increased by delta. In the simulation, delta will be 0.001. This is simply created in Simulink using if-else statements in a 'MATLAB Function' block.

B. Incremental Conductance

Similar to P&O, INC can be programmed using if-else statements in a 'MATLAB Function'. However, it should be more accurate as INC uses the sum of instantaneous conductance (current divided by voltage) and the incremental conductance (change in current divided by change in voltage), which is zero at MPP. These conductance variables are positive to the left of the MPP and negative on the right of the MPP [13] using the P-V curve.

The outline of the INC algorithm is shown as a flowchart by [12] in Fig. 10. Change in voltage ΔV is calculated using the previous stored value of voltage and subtracting it from the new measured voltage, and similarly for change in current ΔI. The duty cycle has an inverse relationship with voltage in the DC converter, so to increase voltage, the duty cycle is decreased.

C. Constant Voltage

The EPS is modified for CV as a MOSFET is connected to the PV. This allows the PV to be connected and disconnected from the DC converter, which allows for measuring the open circuit voltage V_{OC}.

$$V_{ref} = kV_{OC} \tag{10}$$

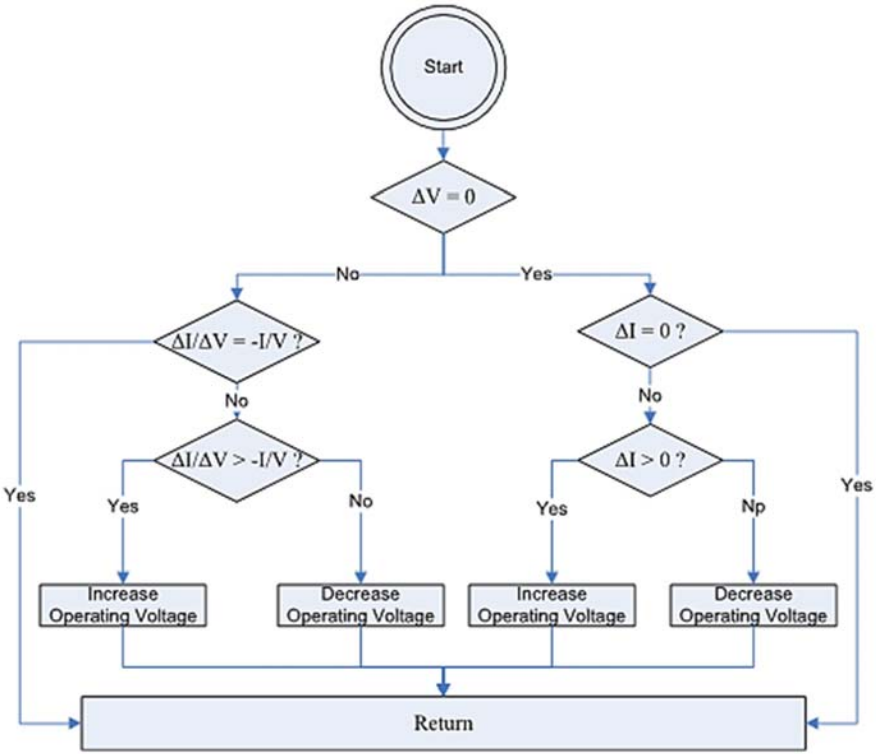

Fig. 10 Flowchart of Incremental Conductance MPPT [12]

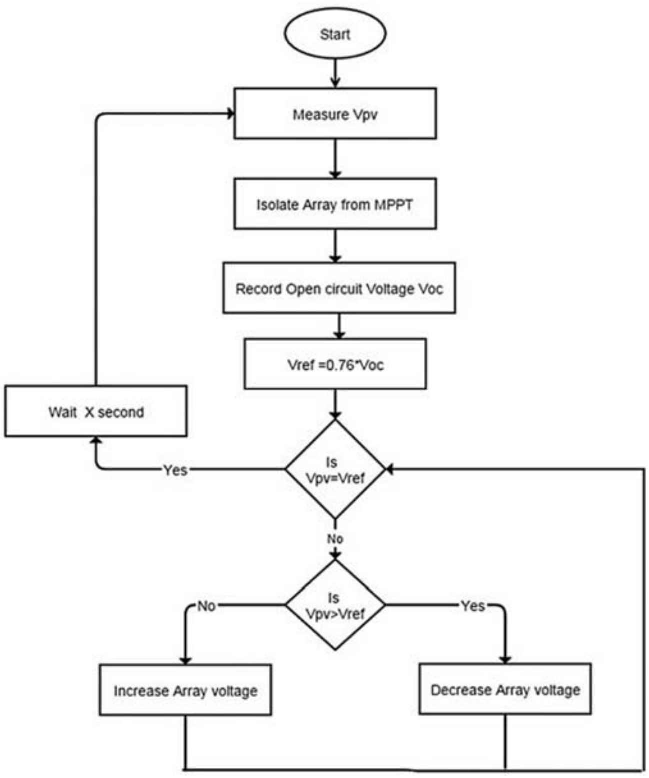

Fig. 11 Flowchart of Constant Voltage MPPT [14]

Given that voltage at MPP V_{ref} is equal to V_{OC} scaled by k as shown in (10), CV can be used to track MPP. This works by disconnecting the PV to make it open circuit and then measure and store V_{OC}. V_{OC} is scaled by k, which will be 0.88, using the PV depicted in Fig. 6, to give V_{ref}. Then, the PV is reconnected to the circuit and the voltage across the PV V_{PV} is measured and compared with V_{REF}. The duty cycle is adjusted to move V_{PV} towards V_{ref}. The cycle will then repeat after pausing for 500 ms in the simulation. This process is depicted in the flowchart by Asim et al. [14] shown in Fig. 11..

D. Fuzzy Logic Control

Fuzzy logic uses linguistic rules to process data similarly to the human brain [15]. The controller processes the inputs using membership functions during fuzzification; assesses if-then rules using a fuzzy inference system (FIS); and provides a precise output through defuzzification.

FLC for MPPT uses the error E and the change in error CE to determine the change in duty cycle which are calculated using (11) and (12) following Kottas et al. [16]:

$$E(k) = \frac{P_{PV}(k) - P_{PV}(k-1)}{i_{PV}(k) - i_{PV}(k-1)} \tag{11}$$

$$CE(k) = E(k) - E(k-1) \tag{12}$$

The value of k represents the current step and k-1 is the previous. Membership functions are used to convert E and CE to linguistic values. These are comprised of five sets: negative big (NB), negative small (NS), zero (ZO), positive small (PS), and positive big (PB).

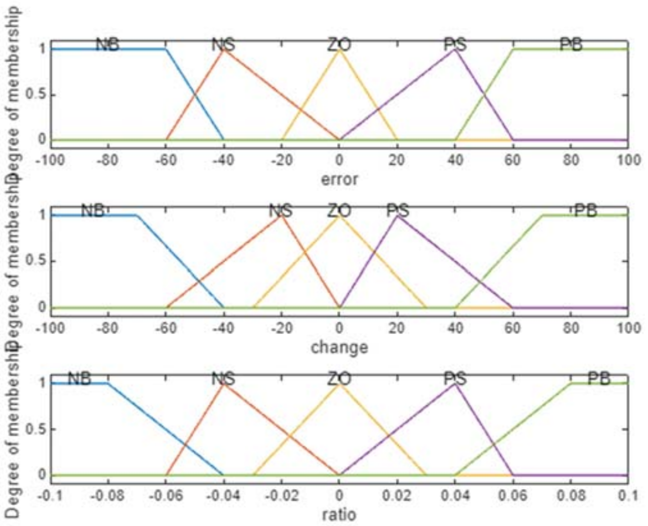

Fig. 12 Membership Functions for Error, Error Change (change) and Duty Change (ratio) for FLC

Fig. 12 illustrates the membership functions for the two inputs, E (error) and CE (change), and the output, change in duty cycle (ratio). This was plotted using MATLAB. The functions were adapted from Fapi et al. [17] using only five sets instead of seven. E and CE are converted to linguistic variables using a Mamdani FIS. The 'Fuzzy Logic Controller' in Simulink processes fuzzy logic and integrates the output to the EPS.

Fuzzy logic rules are used to determine the linguistic value of the change in duty cycle. Five if-then rules were used to determine the value of the change in duty cycle, which is represented in the surface shown in Fig. 13. This figure is generated using the 'gensurf' function in MATLAB using the if-then fuzzy logic rules.

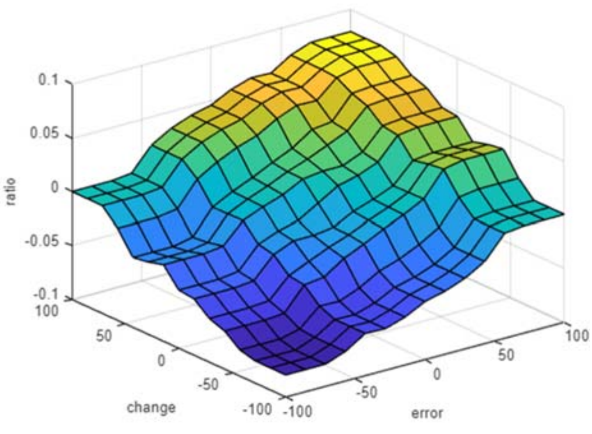

Fig. 13 Fuzzy Inference System Output Surface

E. Particle Swarm Optimization

PSO is another intelligent MPPT method. It is an evolutionary computation based on nature where swarms converge on an optimized solution to a problem [18]. In the case of MPPT, a particle is created at a randomly generated value for duty cycle and the power produced by the PV is stored for the particle. Each particle has a personal best duty cycle and there is a global best duty cycle between all particles. The particles all move with their own velocities and when the algorithm calculates their next velocity to reach the best power output, the particles best, global best and current velocity are all considered [19]. This is demonstrated in Fig. 14.

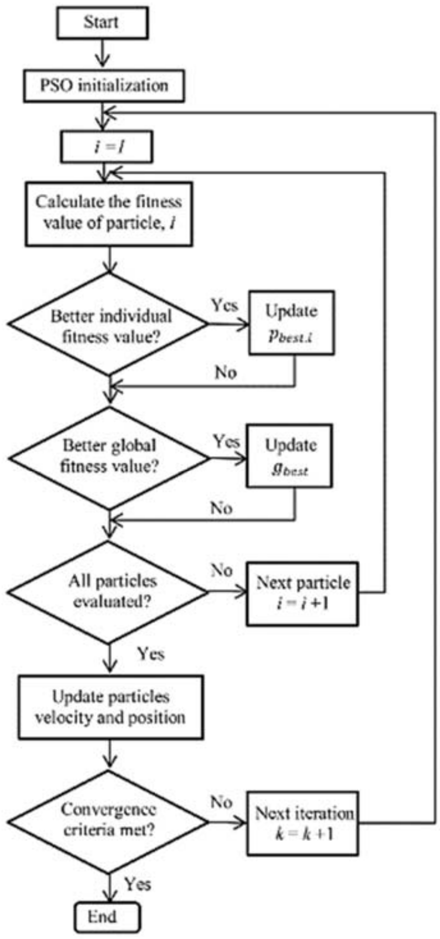

Fig. 14 Particle Swarm Optimization Flowchart [20]

The flowchart shows that the particles continue to recalculate their velocity until convergence is met. This has a negative impact of remaining constant when the conditions of the PV change. This can be resolved by implementing a conventional algorithm with PSO to allow new local MPP to be found [21]. A further flaw with PSO is premature convergence before the true MPP is found.

F. Artificial Neural Network

PV voltage at the MPP can be derived from the temperature using [22]. This is adapted for the simulation as (13):

$$V_{MP} = V_{MP|T_{ref}} + \alpha(T - T_{ref}) \tag{13}$$

V_{MP} is the PV voltage and $V_{MP|Tref}$ is the PV voltage at the MPP for the reference temperature T_{ref}, which will be 25 °C. T is the temperature and α is the temperature coefficient, which will be 0.1%.

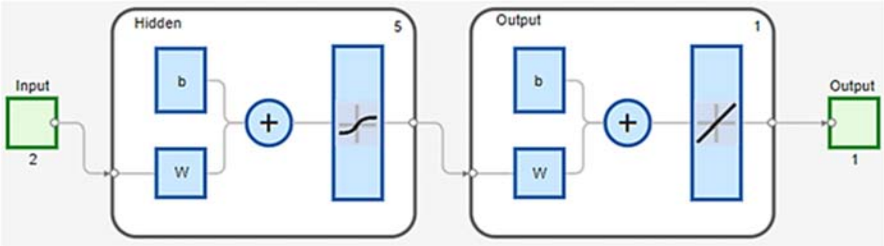

Fig. 15 Artificial Neural Network Model for MPPT

The neural network that will be used for MPPT is a shallow two-layer feedforward network [23]. This network has a hidden layer with five neurons. This model is highlighted using MATLAB in Fig. 15. The inputs to the ANN are the irradiance and temperature of the PV cell [24], so additional temperature and irradiance sensors are needed. The output is the duty cycle that the ANN determines to provide MPP. During training, the ANN will change the weights of its neurons to provide an accurate output [25].

The network was trained offline on randomly generated temperatures and irradiances, and the voltage at MPP is calculated using (13). The model was trained using the Levenberg-Marquardt algorithm with a ratio of 70% training, 15% testing, and 15% validation. The model trained until epoch 283. The ANN was then tested using data it had not been exposed to during training and achieved an average error of 4.54×10^{-8}.

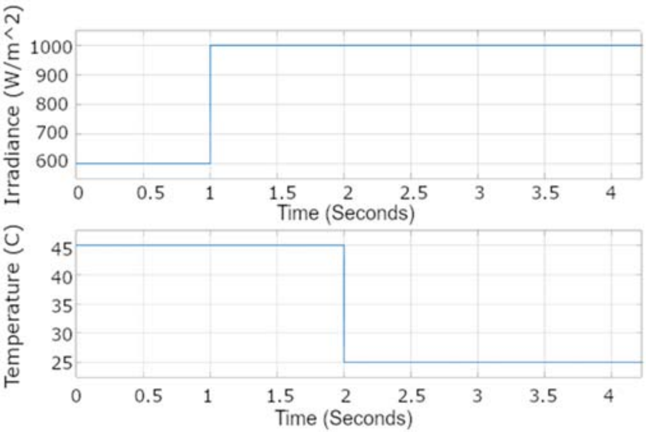

Fig. 16 Irradiance and Temperature Step Functions for ANN Simulation

To test the adaptiveness of ANN for MPPT, two step functions were used to change the conditions for the PV. This is shown in Fig. 16, where irradiance steps up to 1000 Wm^{-2} from 600 Wm^{-2} after one second and temperature steps down from 45 °C to 25 °C after two seconds. Then, irradiance and temperature remain constant.

IV. Results and Analysis

A. Perturb and Observe

The input power and output power for the last 10 seconds of the simulation are highlighted in Fig. 17. The input power remains mostly consistent, with small spikes when the duty cycle changes.

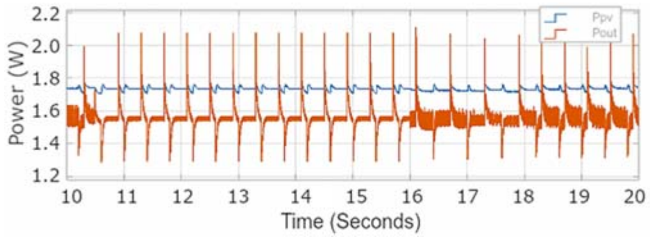

Fig. 17 Input Power (blue) and Output Power (orange) of P&O Simulation over the Last Ten Seconds

The output power has much larger spikes, reaching a peak of 1.76 W, then decreases to its average value. This is the point where the P&O algorithm has found the MPP, but due to the step size, it continuously oscillates around the point. This is clearly demonstrated when looking at the duty cycle over the course of the simulation in Fig. 18.

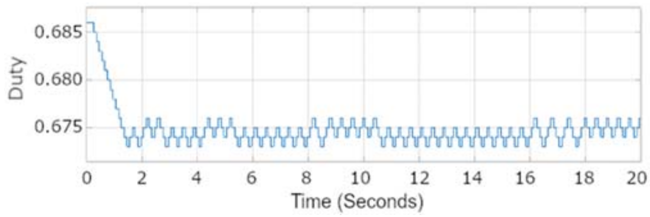

Fig. 18 Duty Cycle During P&O Simulation

The initial duty cycle of the simulation was 0.686, which was the theoretical MPP calculated previously using (1). The duty cycle oscillates in the range of 0.676 and 0.673. The average duty cycle is 0.674, which could be determined as the duty for the MPP using P&O.

The average input power was 1.742 W when using P&O while the output power was 1.537 W. This means the MPPT efficiency was 98.98% using (8) and the efficiency of the boost converter was 88.23% using (9).

B. Incremental Conductance

The input power and output power shown in Fig. 19 is very similar to that of P&O in Fig. 17. The initial duty cycle was 0.686 just like for P&O. The oscillations that occurred in Fig. 20 are very similar to the ones observed in Fig. 18. This suggests that despite INC being a more theoretically accurate MPPT, the performance is equivalent to P&O during the simulation.

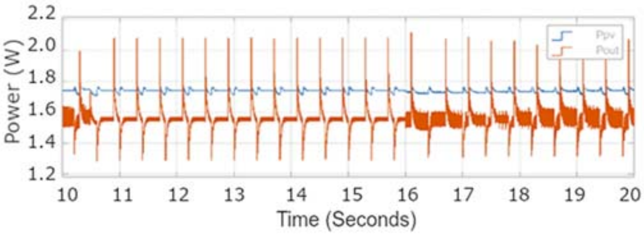

Fig. 19 Input Power (blue) and Output Power (orange) of INC Simulation over the Last Ten Seconds

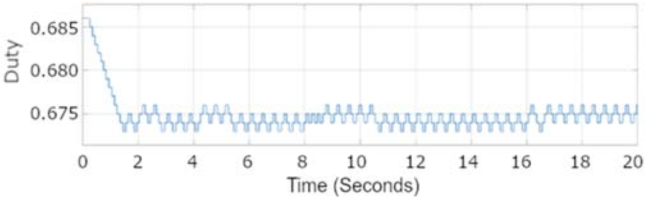

Fig. 20 Duty Cycle During INC Simulation

For INC, the input power was 1.739 W, and the output power was 1.531 W. The MPPT efficiency was 98.81% and the boost converter efficiency was 88.04%.

C. Constant Voltage

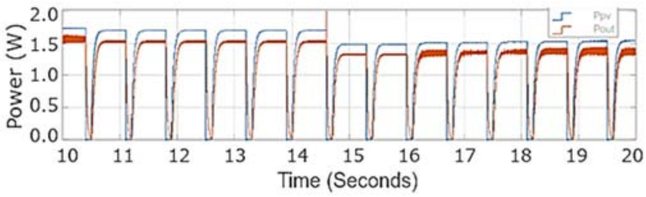

Fig. 21 Input Power (blue) and Output Power (orange) of CV Simulation over the Last 10 Seconds

The PV cell disconnects from the circuit every 500 ms. This causes power losses shown in Fig. 21. There is a similar discrepancy between the input power and output power for the CV simulation when compared to P&O and INC.

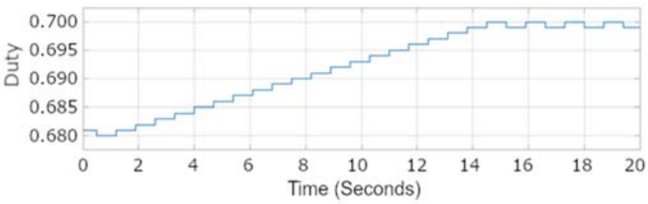

Fig. 22 Duty Cycle During CV Simulation

The initial duty cycle was once again 0.686; however, the CV algorithm determined that the MPP was at a higher duty cycle. The duty cycle increased until reaching 0.7 where the duty cycle oscillates between 0.7 and 0.699.

The input power was 1.739 W and the output power was 1.530 W. The MPPT efficiency was 98.81% and the boost converter efficiency was 87.98%.

D. Fuzzy Logic Control

Fig. 23 shows a similar input power and output power to Figs. 17 and 19. However, the output power spikes are much more frequent.

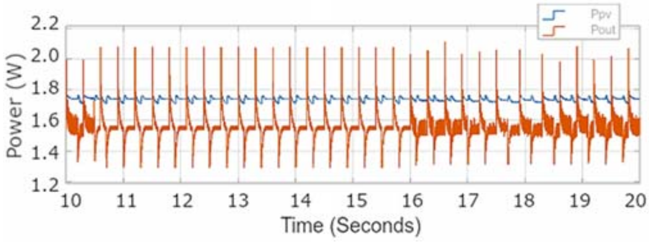

Fig. 23 Input Power (blue) and Output Power (orange) of FLC Simulation over the Last 10 Seconds

The change in duty cycle is shown in Fig. 24. When using FLC, the step is linguistically determined using the membership functions in Fig. 12. The change in duty cycle results in an overstep which needs to be corrected in the subsequent run of the function. This causes a large range of oscillations.

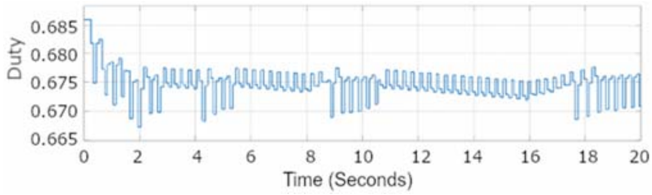

Fig. 24 Duty Cycle During CV Simulation

FLC had an input and output power of 1.739 W and 1.531 W, respectively. This gives an efficiency of 98.81% for MPPT and 88.04% for the boost converter. The MPP duty determined using FLC was 0.675 on average.

E. Particle Swarm Optimization

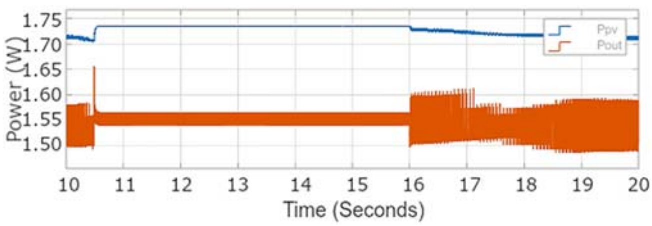

Fig. 25 Input Power (blue) and Output Power (orange) of PSO Simulation over the Last Ten Seconds

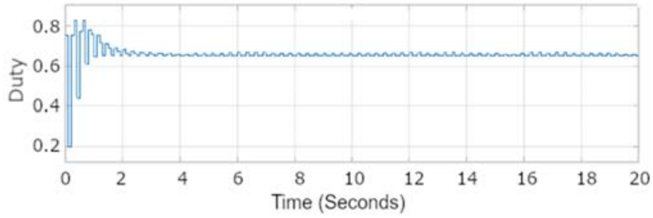

Fig. 26 Duty Cycle During PSO Simulation

Fig. 25 shows a mostly constant input power and an output power which has an oscillation between 1.57 and 1.54 between 10.5 seconds and 16 seconds.

The duty cycle quickly settles after 2 seconds around the MPP as depicted in Fig. 26. Then, duty oscillates between 0.665 and 0.650. The duty cycle is quickly optimized using PSO when compared to conventional MPPT.

For PSO, the input power was 1.710 W with an output power of 1.524 W, providing an MPPT efficiency of 97.16% and a boost converter efficiency of 89.12%.

F. Artificial Neural Network

Fig. 27 shows the power for the ANN simulation. The input power and output power start low around 0.2 W until one second. After one second, the irradiance increases to 1000 Wm^{-2}, which causes an increase in the power to around 0.5 W. Then at two seconds, when the temperature drops to 25 °C, ANN increases the power to 1.7 W for the input and 1.52 W for the output.

The duty cycle is determined using the irradiance and temperature when using ANN. This results in no oscillations since during the simulation these conditions remain constant after two seconds. This is clear in Fig. 28.

In a practical circuit, the power would change due to the small fluctuations of temperature and irradiance. The duty cycle only changes in response to the temperature as shown in Fig. 29. Duty remains constant as the temperature does not change any further after two seconds.

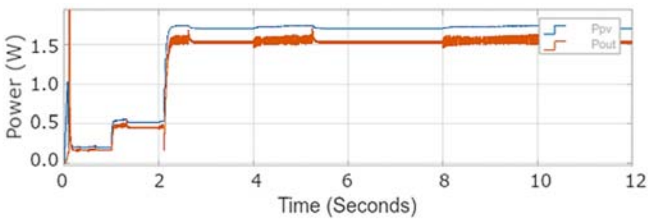

Fig. 27 Input Power (blue) and Output Power (orange) of ANN Simulation

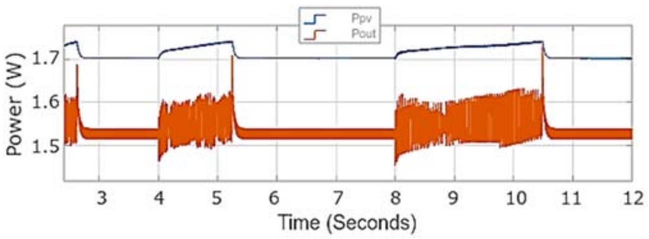

Fig. 28 Input Power (blue) and Output Power (orange) of ANN Simulation over the Last Ten Seconds

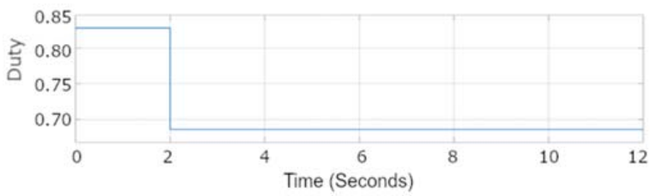

Fig. 29 Duty Cycle During ANN Simulation

ANN produced an input power of 1.735 W and an output power of 1.598W. This gives an MPPT efficiency of 98.58% and a boost converter efficiency of 92.10%.

V. Discussion of MPPT Algorithms

P&O and INC both behave similarly when the MPP is found as the step size is constant. This causes the duty cycle over time to oscillate around the point of maximum power. This step size is a drawback of these methods where both require a long period to reach the required duty cycle for MPP, especially when initial duty and duty at the determined MPPT have a significant difference. Variations of the methods include a variable step size [26], minimizing this issue. The MPP is where the gradient of the curve reaches zero on the P-V graph of the solar cells. As INC calculates the change in power divided by voltage, it is more accurate than P&O. During simulation, P&O resulted with better input and output power than INC. Since P&O and INC are true searching algorithms, duty can be adjusted to maximize the power when the solar module is facing the sun at an angle.

CV has high power wastage due to open circuiting the PV module to measure Voc. This power loss makes it less ideal as an MPPT method. An alternate CV approach is use of a pilot cell, so the solar cells continuously generate power while allowing MPPT. The CV simulation resulted in the same input power as INC but a lower efficiency. Oscillations were also present in this method as well as a long settling time from the initial duty. CV benefits from adjusting duty when the module is not directly facing the sun.

FLC has a wide range of variables which could be tuned to produce great MPPT. Before simulating the circuit, multiple different parameters were tested to produce the final FLC algorithm. The specific ranges used for the membership functions and the rules used for the FIS were determined to be the most suitable for the power converter model. There were very large oscillations in the duty over time. The input power using FLC was the same as CV and INC, and the output power was the same as INC. FLC uses a similar metric to INC to determine the duty cycle, where the error from MPP is calculated and the change in error, which are converted to fuzzy logic. FLC would therefore adapt when the solar cells are facing at an angle to the sun.

PSO additionally has a wide range of variables which can be tuned to change the output behaviour algorithm. However, due to the nature of the particles, it requires a settling time for the particles to converge on the MPP. The particles end up oscillating near the MPP like P&O and INC, however with a much lower step as this is intelligently calculated by each particle. However, PSO also has the drawback of being unable to detect the change in MPP after convergence, which would lead to decreased power output.

For ANN, the network was trained offline using randomly generated temperature and irradiance data using the ideal voltage characteristics of the solar cells. This resulted in a slightly decreased MPP. A better training set for the ANN would be to generate or measure the power of the solar panel for different values of temperature and irradiance, using the circuit in the Simulink model. However, this was not done as a long period of time is required to gather a suitably large sample size. The ANN provided a similar duty cycle to the theoretical duty cycle for MPP which was calculated as 0.686. The input and output power matched that seen when a constant duty cycle was used. ANN can detect when the solar module is at an angle to the sun, since it uses the temperature and irradiance of the cell to calculate the voltage at MPP.

TABLE I
MPPT POWER AND EFFICIENCY COMPARED

MPPT Type	Input Power (W)	Output Power (W)	MPPT Efficiency (%)	DC Converter Efficiency (%)
No MPPT	1.735	1.598	98.58	92.10
P&O	1.742	1.537	98.98	88.23
INC	1.739	1.531	98.81	88.04
CV	1.739	1.530	98.81	87.98
FLC	1.739	1.531	98.81	88.04
PSO	1.710	1.524	97.16	89.12
ANN	1.735	1.598	98.58	92.10

The efficiencies of the MPPT algorithms are summarized in Table I. The average input power with a constant duty cycle (No MPPT) was 1.735 W and the output power was 1.598 W. This gives an MPPT efficiency of 98.58% using (8) and a boost converter efficiency of 92.10% using (9).

The highest input power was generated using the P&O technique, despite the simplicity of the algorithm. This resulted in the highest efficiency for an MPPT technique that was simulated. The highest output power generated by the boost converter was when a constant duty cycle was used, and when an ANN was used to track MPP. This also results in the highest boost converter efficiency when both techniques were simulated.

The lowest input power was generated using the PSO technique and this also resulted in the lowest output power. The PSO algorithm therefore had the lowest MPPT efficiency. However, it did not have the lowest boost converter efficiency as that occurred for CV due to the periodic disconnection of the solar cells from the rest of the circuit.

VI. CONCLUSION

To conclude, ANN is potentially the most accurate MPPT method as it aligns with the theoretical best duty cycle. The ANN MPPT generated 1.735 W from the solar module and therefore has an MPPT efficiency of 98.58% - the highest out of all the methods simulated. The output power of the EPS using ANN was 1.598 W, which is an efficiency of 92.10%. The ANN model could be further improved if the training data were gathered by simulating a multitude of temperature and irradiance conditions using the power converter circuit. This would likely increase the DC converter efficiency.

CV is the worst tracking technique since it lacks active searching of the MPP. However, CV can be utilized in complement with other MPPT techniques when the primary tracking method is unreliable. P&O is another of the better methods according to this study as it had the highest input power of 1.742 W, resulting in an MPPT efficiency of 98.98%. This is further emphasized by the simplicity of the algorithm, requiring less intensive computation. INC has a similar value as it utilizes the P-V characteristics of the solar cells to identify the MPP, which is theoretically more precise. FLC and PSO, while not the best of the algorithms tested, could have high potential accuracy with further tuning to fully optimize them.

Overall, ANN is the best MPPT algorithm for the EPS of a CubeSat when considering both MPPT efficiency and boost converter efficiency. This paper recommends the use of ANN for MPPT after consideration of all the simulations completed. Additionally, further optimization for PSO and FLC could be considered as a competitor to the ANN.

REFERENCES

[1] K. Diaz, A. Toorian and S. Lee, “The CubeSat Approach to Space Access,” in 2008 IEEE Aerospace Conference, Big Sky, 2008.
[2] S. Lee, “CubeSat Information,” February 2022. (Online). Available: https://static1.squarespace.com/static/5418c831e4b0fa4ecac1bacd/t/62193b7fc9e72e0053f00910/1645820809779/CDS+REV14_1+2022-02-09.pdf. (Accessed March 2025).
[3] A. Ali, M. R. Mughal, H. Ali and L. Reyneri, “Innovative power management, attitude determination and control tile for CubeSat standard NanoSatellites,” Acta Astronautica, vol. 96, pp. 116-127, 2014.
[4] J. M. Álvarez, D. Alfonso-Corcuera, E. Roibás-Millán, J. Cubas, J. Cubero-Estalrrich, A. Gonzalez-Estrada, R. Jado-Puente, M. Sanabria-Pinzón and S. Pindado, “Analytical Modeling of Current-Voltage Photovoltaic Performance: An Easy Approach to Solar Panel Behavior,” Applied Sciences, vol. 11, no. 9, p. 4250, 2021.
[5] S. A. Khan, A. Ali, T. Mustafa and Z. Tao, “Efficient Power Conditioning: Enhancing Electric Supply for Small Satellite Missions,” Aerospace, vol. 11, no. 11, p. 920, 2024.
[6] N. Karami, N. Moubayed and R. Outbib, “General review and classification of different MPPT Techniques,” Renewable and Sustainable Energy Reviews, vol. 68, pp. 1-18, 2017.
[7] C. Moler. MATLAB. (2024). MathWorks. Accessed: January 2025. (Online). Available: https://uk.mathworks.com/products/matlab.html
[8] CESI S.p.A., “Datasheet CTJ-30,” 2020. (Online). Available: https://www.cesi.it/app/uploads/2020/03/Datasheet-CTJ30-1.pdf. (Accessed 11 March 2025).
[9] EnduroSat, “1U SOLAR PANEL X/Y,” (Online). Available: https://www.endurosat.com/products/1u-solar-panel-x-y/. (Accessed 12 March 2025).
[10] D. W. Hart, Power Electronics, McGraw-Hill Education, 2010, pp. 211-220.
[11] M. Engelhardt. LTspice. (2024). Analog Devices. Accessed: October 2024. (Online). Available: https://www.analog.com/en/resources/design-tools-and-calculators/ltspice-simulator.html
[12] D. Verma, S. Nema, A. M. Shandilya and S. K. Dash, “Comprehensive analysis of maximum power point tracking techniques in solar photovoltaic systems under uniform insolation and partial shaded condition,” Journal of Renewable and Sustainable Energy, vol. 7, no. 4, p. 42701, 2015.
[13] B. Liu, S. Duan, F. Liu and P. Xu, “Analysis and Improvement of Maximum Power Point Tracking Algorithm Based on Incremental Conductance Method for Photovoltaic Array,” in 2007 7th International Conference on Power Electronics and Drive Systems, Niagara Falls, 2007.
[14] M. Asim, M. Tariq, M. Mallick, I. Ashraf, S. Kumari and A. K. Bhoi, “Critical Evaluation of Offline MPPT Techniques of Solar PV for Stand-Alone Applications,” in Advances in Smart Grid and Renewable Energy, Springer, 2018, pp. 13-21.
[15] R. K. Rai and O. P. Rahi, “Fuzzy Logic based Control Technique using MPPT for Solar PV System,” in 2022 First International Conference on Electrical, Electronics, Information and Communication Technologies (ICEEICT), 2022.
[16] T. L. Kottas, Y. S. Boutalis and A. D. Karlis, “New maximum power point tracker for PV arrays using fuzzy controller in close cooperation with fuzzy cognitive networks,” IEEE Transactions on Energy Conversion, vol. 21, no. 3, pp. 793-803, 2006.
[17] C. B. N. Fapi, H. Tchakounté, M. Ndje, P. Wira, D. O. Abdeslam, M. Louzazni and M. Kamta, “Fuzzy Logic Based Maximum Power Point

Tracking Control for Photovoltaic Systems: A Review and Experimental Applications," Archives of Computational Methods in Engineering, 2024.
[18] A. Khare and S. Rangnekar, "A review of particle swarm optimization and its applications in Solar Photovoltaic system," Applied Soft Computing, vol. 13, pp. 2997-3006, 2012.
[19] M. Abdulkadir, A. H. M. Yatim and S. T. Yusuf, "An Improved PSO-Based MPPT Control Strategy for Photovoltaic Systems," International Journal of Photoenergy, no. 1, 2014.
[20] A. K. Podder, N. K. Roy and H. R. Pota, "MPPT methods for solar PV systems: a critical review based on tracking nature," IET Renewable Power Generation, vol. 13, no. 10, pp. 1615-1632, 2019.
[21] K. Ishaque, Z. Salam, M. Amjad and S. Mekhilef, "An Improved Particle Swarm Optimization (PSO)–Based MPPT for PV with Reduced Steady-State Oscillation," IEEE Transactions on Power Electronics, vol. 27, no. 8, pp. 3627-3638, 2012.
[22] E. Cuce, P. M. Cuce, I. H. Karakas and T. Bali, "An accurate model for photovoltaic (PV) modules to determine electrical characteristics and thermodynamic performance parameters," Energy Conversion and Management, vol. 146, pp. 205-216, 2017.
[23] A. Anzalchi and A. Sarwat, "Artificial neural network based Duty Cycle estimation for maximum Power Point tracking in Photovoltaic systems," in SoutheastCon 2015, 2015.
[24] L. P. N. Jyothy and M. R. Sindhu, "An Artificial Neural Network Based MPPT Algorithm for Solar PV System," in 2018 4th International Conference on Electrical Energy Systems (ICEES), 2018.
[25] T. A. Ocran, J. Cao, B. Cao and X. Sun, "Artificial neural network maximum power point tracker for solar electric vehicle," Tsinghua Science and Technology, vol. 10, no. 2, pp. 204-208, 2005.
[26] A. Al-Diab and C. Sourkounis, "Variable step size P&O MPPT algorithm for PV systems," in 2010 12th International Conference on Optimization of Electrical and Electronic Equipment, 2010.